Journal of Non-Crystalline Solids 466–467 (2017) 58–63

Contents lists available at ScienceDirect

Journal of Non-Crystalline Solids

journal homepage: www.elsevier.com/locate/jnoncrysol

RGB emission of Mn^{2+} doped zinc phosphate glass

H. Félix-Quintero[a,b,*], I. Camarillo-Garcìa[c], J. Hernández-Alcántara[b], E. Camarillo-García[b], A. Cordero-Borboa[b], C. Flores-Jiménez[b], M. García-Hipólito[d], F. Ramos-Brito[e], D. Acosta-Najarro[b], H. Murrieta-Sánchez[b]

[a] Posgrado en Ciencia e Ingeniería de Materiales, Universidad Nacional Autónoma de México, AP 70-360, Coyoacán 04510, DF, Mexico
[b] Instituto de Física, Universidad Nacional Autónoma de México, AP 20-364, Álvaro Obregón 01000, DF. Mexico
[c] Universidad Autónoma Metropolitana, Unidad Iztapalapa, División de Ciencias Básicas e Ingeniería, San Rafael Atlixco 186, 09340, DF, Mexico
[d] Instituto de Investigaciones en Materiales, Universidad Nacional Autónoma de México, AP 70-360, Coyoacán 04510, DF, Mexico
[e] Laboratorio de Síntesis de Materiales, Facultad de Ciencias Físico-Matemáticas, Universidad Autónoma de Sinaloa, Ciudad Universitaria S/N 80000, Culiacán de Rosales, Sinaloa, Mexico

ARTICLE INFO

Keywords:
Mn^{2+}
Zinc phosphate glass
ZnO
RGB luminescence

ABSTRACT

We report the photoluminescence (PL) of Mn^{2+} doped zinc phosphate glass as melted. Raman, X-Ray diffraction (XRD), Energy-Dispersive X-ray Spectroscopy (EDS) were used to get a better characterization. During the synthesis process, the Mn^{2+} ions, tetrahedrally coordinated ($^{IV}Mn^{2+}$) in the glass, partially precipitate on octahedral sites ($^{VI}Mn^{2+}$) that gives place to the simultaneous occurrence of green and red luminescence, due to the spin-forbidden $^4T_1(G) \rightarrow {}^6A_1(S)$ and $^4T_{1g}(G) \rightarrow {}^6A_{1g}(S)$ transitions in $^{IV}Mn^{2+}$ and $^{VI}Mn^{2+}$ respectively. The ratio $^{IV}Mn^{2+}/{}^{VI}Mn^{2+}$ can be controlled by the increase of %Mn in the glass and, hence, the ratio between green and red emissions can be controlled. The change of Mn^{2+} ions coordination form 4 to 6 is seen by Electron Paramagnetic Resonance (EPR) and lifetime measurements. PL results indicate the precipitation of crystalline ZnO phases with relatively small particle size that produces its characteristic blue emission due to conduction band to valence band exciton transitions. The transition $^6A_1(S) \rightarrow {}^4E(D)$ of Mn^{2+} centered at 350 nm can produce a blue and red dual luminescence by the overlap with the valence band to conduction band transition of ZnO, while the transition $^6A_1(S) \rightarrow {}^4A_1(G)$ of Mn^{2+} centered at 409 nm produces the green and red dual luminescence that is dependent on %Mn in the glass.

1. Introduction

Recently a great attention has been paid to the development of new phosphors that can be excited with UV and blue electromagnetic radiation due to the purpose to increase the efficiency in white light-emitting solid state devices. Glasses containing transition metal ions are of special interest due to their electrical [1–5], optical [6–13] and magnetic properties [14,15] that makes them suitable for many applications in fields like electronics [4,5], catalysis [16,17] and magnetic information storage [14,18]. These properties arise from the presence of transition metal ions in different valence states [3,19,20]. Then for applications as white light-emitting solid state devices transition metal ions are very good candidates for this purpose. Mn^{2+} doped phosphate glasses are especially attractive as red phosphor materials due to their high transparency. As for the most d-d transitions in transition metal ions, PL from Mn^{2+} centers ($[Ar]3d^5$) strongly depends on ligand field strength and may occur over the spectral range from deep green to far red [21,22,23]. The corresponding excitation spreads the spectral range from about 300 to 500 nm with excitation bands typically centered at: 350, 360, 410, 420 and 500 nm, corresponding to the transitions of $^6A_1(S) \rightarrow {}^4T_1(P)$, $^6A_1(S) \rightarrow {}^4E(D)$, $^6A_1(S) \rightarrow {}^4T_2(D)$, $^6A_1(S) \rightarrow \{{}^4A_1(G), {}^4E(G)\}$ and $^6A_1(S) \rightarrow {}^4T_2(G)$, respectively [24]. Although emission spectra are usually characterized by a broad band, two principal cases may be distinguished: if Mn^{2+} ions are incorporated in tetrahedral neighborhood the respective emission typically occurs in the green spectral range, on the other hand, if their coordination environment is octahedral the emission lies in the orange-red spectral range. Consequently, for matrices within which Mn^{2+} could precipitate simultaneously on both types of lattice sites, dual-mode luminescence can be generated [24,25]. The content of existing manganese in both coordinations in the glass depends on the quantitative properties of modifiers such as: glass precursors, size of the ions in the glass structure, their field strength, etc. [26]. Because Mn^{2+} ions are paramagnetic, also show EPR absorptions at room temperature.

* Corresponding author at: Posgrado en Ciencia e Ingeniería de Materiales, Universidad Nacional Autónoma de México, AP 70-360, Coyoacán 04510, DF, Mexico.
E-mail address: h.felix@fisica.unam.mx (H. Félix-Quintero).

http://dx.doi.org/10.1016/j.jnoncrysol.2017.04.002
Received 20 February 2017; Received in revised form 6 April 2017; Accepted 8 April 2017
Available online 17 April 2017

Usually, the spectra consist of resonance lines centered at g = 2.0, 3.3 and 4.3 with their relative intensity being strongly dependent on Mn^{2+} concentration [27].

This work deals with the RGB luminescence of Mn^{2+} doped zinc phosphate glass as melted and as the manganese ion concentration varies in the range 0–12%. The high quantum efficiency of Mn^{2+} red emission has already been reported in phosphate glasses [28]. In addition, during the synthesis process of zinc phosphate glasses ($Zn_3(PO_4)_2$), zinc oxide (ZnO) nano-crystalline species can be produced giving place to its characteristic blue emission. In order to gain a better characterization, other techniques were applied such as EDS, Raman spectroscopy, hardness measurements, EPR and XRD.

2. Materials and methods

Zinc phosphate glasses were synthesized in wet phase by chemical etching of metallic Zn and liquid acid H_3PO_4 and heated at 70 °C until all H_2 gas goes to the atmosphere, then the solution was dried at 90 °C. In order to dope this resulting powder a well dried MnO powder was mixed and milled in the amounts calculated for obtaining glasses at each molar composition given as 0, 0.4, 1, 2, 5, 8 and 12%, named as, A, B, C, D, E, F and G, respectively. Each resulting powder was melted at 1100 °C in an alumina crucible at ambient atmosphere for 2 h in a Muffle furnace Felisa FE 340 and solidified in a cooper mold at room temperature. All samples were transparent, uncolored and hygroscopic, only the G sample became purple due to the high manganese concentration.

Absorption spectra were obtained from a Cary 5000 UV–Vis-NIR spectrometer in 200–900 nm spectral range for all samples. Excitation and emission spectra were obtained in a Perkin Elmer LS 55 fluorescence spectrometer, the former in 300–500 nm and the latter in 400–700 nm spectral ranges for all samples. Lifetime measurements were carried out with an HP Infinium oscilloscope, exciting the glass with a 5 W 450 nm laser source and collecting the luminescence with an ACTON SpectraPro 2500i monochromator using a SR530 lock-in amplifier from Stanford Research Systems for all samples. Raman spectra were measured in a Thermo Scientific DXR Raman Microscope from 400 to 1600 cm^{-1} for A, B, C and G samples. XRD pattern was obtained from a Kristalloflex Diffraktometer D5000 from 2θ = 15 to 70 with a speed of 5 s each 0.02 degrees for B sample. EDS analysis was obtained with a Leica Cambridge Stereoscan 330 Scanning Electron Microscope (SEM) for B (0.4% Mn) and G (12% Mn) samples. EPR measurements were obtained in a JEOL JES-RE3X ESR spectrometer using a frequency of 9.12 GHz, with a 100 KHz frequency modulation, and a magnetic field strength of 330 ± 250 mT to cover the whole spectrum. All measurements were made at room temperature. Hardness measurements were done through the scratch resistance of the glass to various materials.

3. Results and discussion

The elementary chemical glass composition was obtained by EDS analysis technique that shows that these glasses have an average composition of: 60.81% O, 12.06% P and 27.11% Zn, this could correspond to chemical formula $Zn_3(PO_4)_2$ with an excess of both zinc and oxygen ions. When MnO is added, the Mn^{2+} ions replace the Zn^{2+} ions, this could create the necessary conditions for the oxidation of Zn with the oxygen generated from the dissociation of MnO. The hardness of the glass is from 4 to 5 in Mohs scale.

Fig. 1 shows the Raman spectra as a function of manganese concentration. These spectra are characteristic of metaphosphate glasses as are shown in the respective references [29,30,31]. The main features in the spectra are as follow: the $(PO_2)_{asym}$ band at 1251 cm^{-1}, the $(PO_2)_{sym}$ band at 1206 cm^{-1}, the $(POP)_{sym}$ band at 703 cm^{-1} and a band at 310 cm^{-1}, that also appear in the doped samples, although their intensity decreases as the Mn^{2+} concentration increases. It should

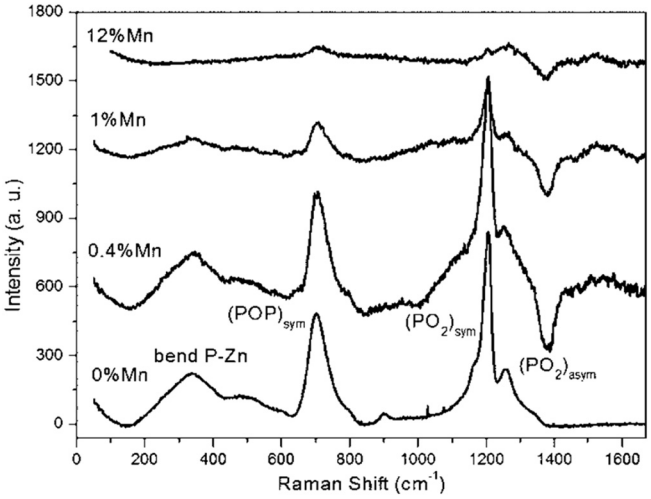

Fig. 1. Raman spectra of the zinc phosphate glass as a function of Mn^{2+} ion concentration showing four bands and its decrease as the Mn concentration increases meaning the reduction of all vibrational modes by the deformation of the glass.

be mentioned that the last band has been associated as a bend mode of phosphate polyhedral with a Zn modifier [29]. On the other hand, these spectra results quite similar to the Raman spectra of the glasses $xZnO(1-x)P_2O_5$ with $0 < x < 0.5$ and high mol% of ZnO [29]. The reduction of the bands intensity when %Mn increases means a reduction of all vibrational modes, that could be due to the glass deformation by the addition of an impurity [31] and the necessary power decrease of the incident laser because the strong absorption bands of the Mn^{2+} in the visible region.

The XRD for the phosphate glass for B (0.4% Mn) sample is shown in Fig. 2. It consists of a broadband which is characteristic of amorphous materials, and no other peaks of crystalline phases were observed. Considering that the Scherrer equation states that for a grain size of a crystal < 10 nm the FWMH of the XRD peak will be relatively wide so that it's improbable to be observed. However, it can be seen a relatively small band, barely noticeable, bellow the XRD of the glass, located where the greatest intensity lines of the XRD pattern would appear for ZnO and ZnO_2. Although at this point it is not clear enough to suggest that if ZnO possible nano-particles are present, they will have a grain size lower than 10 nm. Later, the optical measurements of the glasses might reinforce this proposal.

Fig. 3, shows the absorption spectra of the glass from 350 to 700 nm as a function of MnO concentration. In this figure the main feature is a band in the UV region due to Mn^{2+} ions which is centered at 409 nm

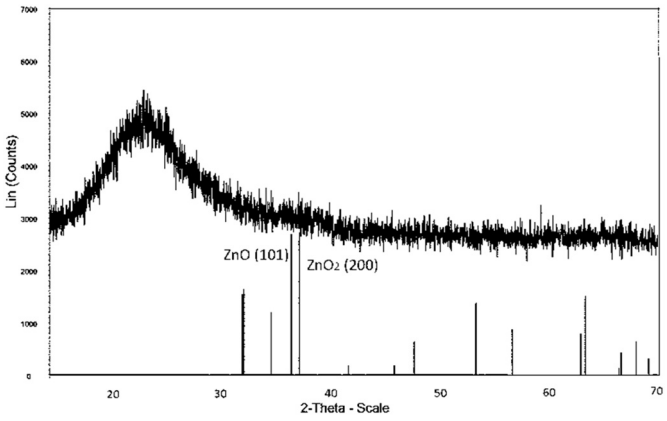

Fig. 2. XRD of the zinc phosphate glass with 0.4% MnO consisting of a broad band characteristic of amorphous materials and a barely noticeable band right of the first one. Below are the XRD patterns of crystalline ZnO and ZnO_2 suggesting the possible presence of ZnO.

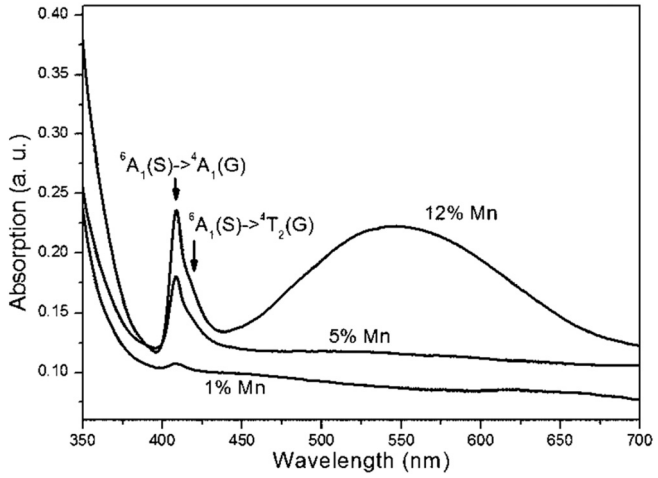

Fig. 3. Absorption spectra of the zinc phosphate glass as a function of Mn^{2+} concentration showing the two principal absorption bands at 409 and 415 nm and a broadband band in the VIS region happening by the high content of Mn.

corresponding to the $^6A_1(S) \rightarrow {}^4A_1(G)$ transition. Also it should be noticed a shoulder around 415 nm due to the transition $^6A_1(S) \rightarrow {}^4E(G)$. These electronic transitions are spin-forbidden, but they might be favored due to the distortion in the short range of the coordination environment. When Mn ions concentration is as high as 12%, a broadband appears in the VIS range at 540 nm due to the transition $^6A_1(S) \rightarrow {}^4T_2(G)$, which might be happening due to mutual perturbation among Mn ions from nearby structures forming pairs, for instance, such as a couple of octahedral-tetrahedral neighbors. The possible presence of ZnO particles might also raise other interaction or perturbation of Mn optical centers.

The glasses PL emission spectra, at the wavelength excitation of 409 nm, are shown in Fig. 4.a for three different concentrations, D (2%), E (5%) and G (12%). The main feature is a complex broadband in the range from 450 nm to 750 nm. A broadband peaking at 515 nm and another broadband peaking at 570 nm for samples D and E, and a dominating broadband at 607 nm when the concentration of Mn^{2+} is equal to 12%, are the overlapping bands composing the broad one. When Mn^{2+} ion concentration increases there are changes in the coordination around manganese ions, i. e., from tetrahedral to octahedral, which causes deep effects such as the observed red shift, the reduction of the green band intensity and the increase of yellow-orange emission band [23,32].

Fig. 4.b shows the glasses excitation spectra which were taken with a wavelength emission at 600 nm and for two manganese concentrations, 5% and 12% (E and G samples). The complex excitation spectra consists of bands centered at 348, 360, 409 and 424 nm that are ascribed to the transitions $^6A_1(S) \rightarrow {}^4E(D)$, $^6A_1(S) \rightarrow {}^4T_2(D)$, $^6A_1(S) \rightarrow {}^4A_1(G)$ and $^6A_1(S) \rightarrow {}^4T_2(G)$ respectively [24]. With respect to the other samples, the excitation spectra are quite similar to those already given.

On other respect, when the excitation wavelength varies from 409 (Fig. 4.c) to 425 nm, there are modifications among emission intensities. Both bands, green and yellow-orange intensities decreases and in addition, a redshift of yellow-orange emission band is observed by the increase of excitation wavelength as shown in Fig. 4.c.

The excitation spectrum that gives rise to the green emission is similar to the one shown in Fig. 4.b, however in this case the maximum excitation band is slightly red shifted, from 409 to 413 nm, the comparison between excitation bands that gives rise to green and yellow-orange emission bands is shown in inset of Fig. 4.b, the red shift of the excitation band is due to the difference of ligand fields of both tetrahedral and octahedral symmetries. When the excitation wavelength is 490 nm the green emission band vanishes and the yellow-

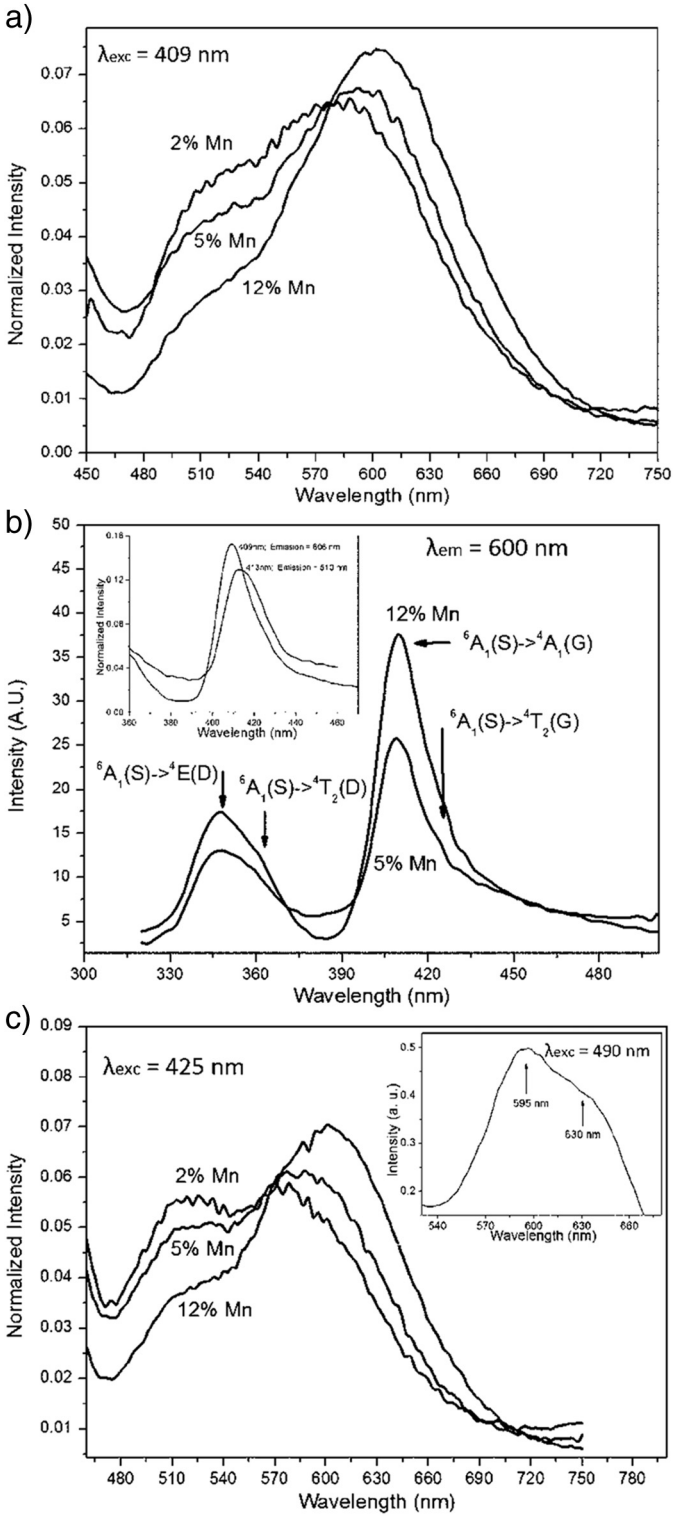

Fig. 4. a) Mn^{2+} doped zinc phosphate glass PL emission spectra at the wavelength excitation of 409 nm for three concentrations where can be seen a green-yellow dual PL and a red shift of yellow PL as the Mn concentration increase. b) Excitation spectra with a wavelength emission at 600 nm for two Mn^{2+} concentrations showing four excitation bands. In inset is the comparison between the excitation spectrum that gives rise to red and green PL emissions. c) PL emission spectra at the wavelength excitation of 425 nm for three concentrations. In inset is the PL emission spectrum when the wavelength excitation is increased to 490 nm, as can be seen the green emission is absent and the orange band looks composed by yellow and red bands.

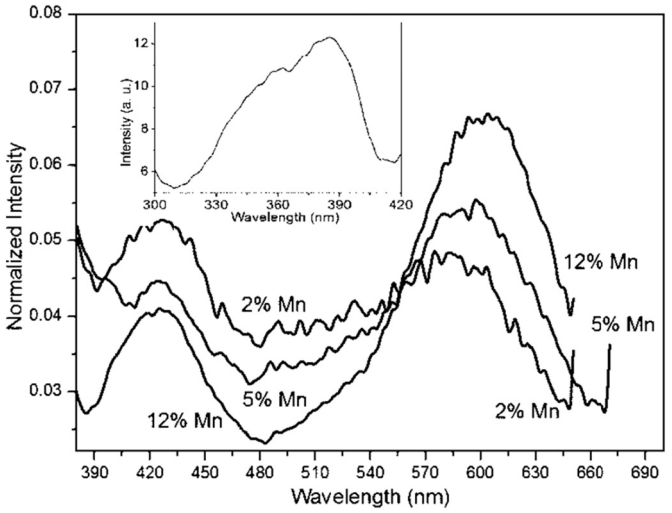

Fig. 5. Mn^{2+} doped zinc phosphate glass PL emission spectra at the wavelength excitation of 350 nm for three concentrations showing a blue-red dual luminescence. The blue emission arises from the presence of ZnO. In inset is the excitation scheme that gives rise to the blue emission corresponding to the excitation band of ZnO.

orange emission looks composed by two wide bands: a yellow emission band centered at 595 nm and an orange band centered at 630 nm as can be seen in inset of Fig. 4.c.

Fig. 5 shows the emission spectra when the high energy band centered at 350 nm shown in Fig. 4.b is excited. This shows a double broad band: a blue emission band centered at 430 nm, and a yellow-orange band centered around 590 nm, but it should be noticed that the green emission is absent. The excitation scheme that gives rise to the blue emission is shown in inset of Fig. 5. The blue emission and his corresponding excitation band are very similar to that reported for crystalline zinc oxide with the emission arising from the transition of the conduction band to valence band and exciton type transitions [33–37]. This result, altogether with Raman and X-Ray diffraction spectra suggest that is highly probable that ZnO crystalline nano-species are created during the synthesis process of the zinc phosphate glass. Although this is an important result, this will be studied in detail in a forthcoming work with an induced ZnO crystalline phase growth as well as the formation of ZnO defects (that gives place to a broad visible emission [33]) and its role in this kind of zinc phosphate glass.

Fig. 6.a shows the PL spectra of the glass when exciting with a 5 Watt 450 nm laser for the B, E and G samples. This figure presents the wide Mn^{2+} emission spectra from 470 to 700 nm which is composed by three bands peaking at 510, 570–600 and 646 nm, this last band has already been shown before in Fig. 4.c, but in that case, the distinction between the yellow and red emission bands as seen in inset of Fig. 4.c is better resolved, these differences between Fig. 6.a and Fig. 4.c arise from the power of excitation source, detectors sensibility and the corrections made by the software employed. The $Zn_3(PO_4)_2$ consist of spiral chains or alternating phosphate and zinc tetrahedron running parallel to the twofold screw axis, these chains are interconnected by a second set of zinc tetrahedral [38]. C.E. Smith and R.K. Brow [31] have reported that the change of ZnO for MgO in zinc phosphate glass has important changes in some physical properties and structure of the glass, although Zn and Mg have very similar sizes. The ionic size of Mn^{2+} is slightly lower with respect to that of Zn^{2+}, therefore the substitution of Zn for Mn will have the same kind of consequences and the oxygen excess detected by EDS and the presence of ZnO will distort the glass structure as was revealed by the Raman spectra. When Mn^{2+} enters substitutional instead of Zn^{2+}, in principle, it will enter as four coordinated. It is clear that when the Mn concentration is low the four coordination is more favorable, giving place to a relatively sharp green emission and a low yellow-orange emission. When the

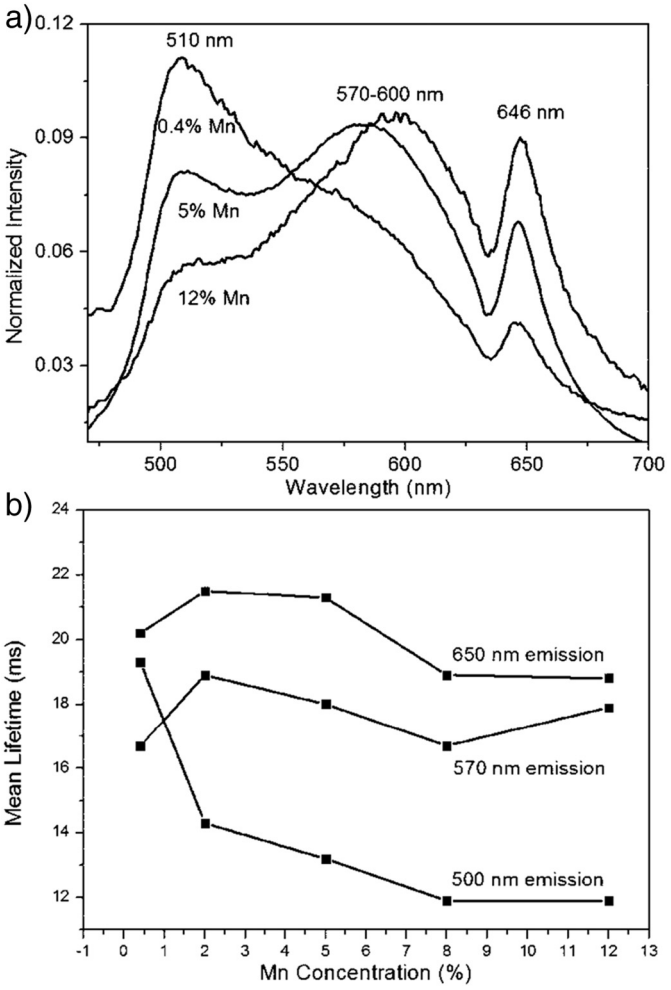

Fig. 6. a) Mn^{2+} doped zinc phosphate glass PL emission spectra exciting with a 5 Watt 450 nm laser for three concentrations. The emission is composed by three bands, the green band corresponding to a 4 coordinated Mn^{2+} ions, the yellow one to Mn^{2+} ions in a distorted octahedral symmetry and the red one to a 6 coordinated Mn^{2+} ions. b) Mean lifetime measurements of the three principal peaks of Fig. 6.a as a function of Mn concentration.

Mn^{2+} concentration increases and so the oxygen excess, the ligands around Mn^{2+} ions will be slowly changed from tetrahedral to an octahedral symmetry that gives place to the emission that shifts from green to red. Some of these Mn^{2+} ions will enter six coordinated in the distorted glass giving place to the red emission centered at 648 nm. This can be confirmed with the mean lifetime measurements shown in Fig. 6.b for the three principal peaks observed as a function of Mn concentration. The average mean lifetimes are 14.12, 17.64 and 20.14 ms for 500, 570 and 650 nm emissions, respectively. The overlap between 500 and 570 nm emissions lifetime when Mn concentration is low tell us that both emissions arise from a similar symmetry giving more information that the 570 nm emission is from a distorted tetrahedral symmetry. This overlap between 500 and 570 nm emissions lifetime vanishes when Mn concentration increases, because at higher content the symmetry around Mn^{2+} ions is a possible octahedral coordination. At the higher Mn concentration the 570 and 650 nm emissions lifetimes become closer, again because the 570 nm emission arise from an even more apparent octahedral symmetry due to a higher glass structure distortion.

EPR measurements were made in order to acquire a better knowledge of the local structure of the Mn^{2+} ions surroundings into the glasses.

Structural disorder is a characteristic feature of the vitreous state.

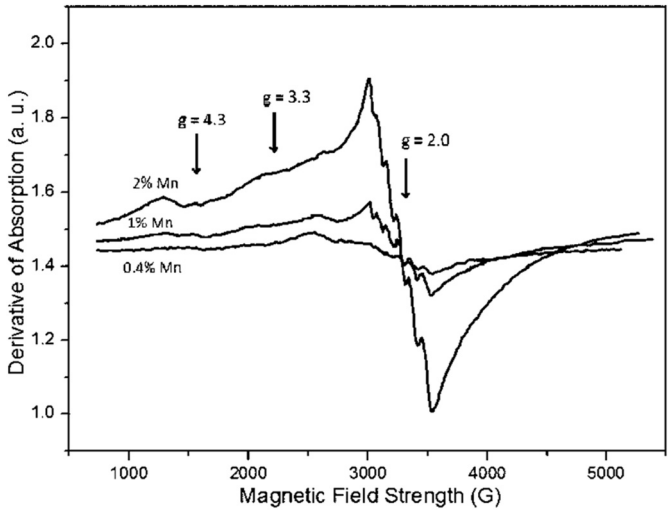

Fig. 7. Mn^{2+} doped zinc phosphate glass EPR spectra as a function of Mn^{2+} concentration. It consists mainly of three resonances centered at 2.0, 3.3 and 4.3 with characteristics that indicate the presence of Mn^{2+} in both tetrahedral and octahedral symmetries that depends on Mn concentration.

Local environments of paramagnetic ions in glasses are subject to random distortions and random orientations of magnetic axes when a magnetic field is applied. This result in substantial distributions of the spin-Hamiltonian parameters, which for Mn^{2+} are the tensors D and E related through the spin-Hamiltonian [39]:

$$H = g\beta B \cdot S + (1/3)D[3S^2z - S(S+1)] + E(S^2x - S^2y)$$

which are related to the manganese ion local symmetry, a distorted octahedral/tetrahedral symmetry and a rhombic symmetry. It is well known that the g tensor for Mn^{2+} ions is isotropic and the possible observations of the spin allowed transitions [39]: $|S = \pm 5/2> \rightarrow |S = \pm 3/2>$, $|S = \pm 3/2> \rightarrow |S = \pm 1/2>$ and $|S = +1/2> \rightarrow |S = -1/2>$, depends on the relative magnitude of these interactions.

Indeed, the resonance magnetic fields for the noncentral fine-structure transitions contain the terms linear in D and E which vanish for the central fine-structure transition. Therefore the parameter distributions smear out all the noncentral transition lines in glasses, i.e. these might be observed as shoulders on the sides of the central $|S = +1/2> \rightarrow |S = -1/2>$ transition which is of the derivative type [40]. There are other interactions that also contribute to the widening of the ESR lines such as the concentration dependent spin-spin interaction. All of these features were observed in the present work as will be shown below.

The Fig. 7 shows the EPR spectra as a function of the Mn^{2+} ions concentration: 0.4, 1, and 2%Mn. The Mn^{2+} EPR spectra are sensitive to the local symmetry in the glass network, as mentioned before, and in addition, give us information about the valence states and interactions. As can be seen from this figure, there is a strong dependence of the absorption spectra with the structure surrounding the Mn^{2+} ion and the manganese samples content. The EPR spectra consist mainly of some features such as absorption bands or resonances labeled as g = 2.0, 3.3 and 4.3. The resonance at g = 2.0 is attributed to Mn^{2+} ions in octahedral/tetrahedral symmetry environments, and is known to arise from the transition between the energy levels of the Kramer's doublet $|\pm 1/2>$ [27,41,42]. The wide of the band is due to the contribution of manganese ions in octahedral and tetrahedral symmetries and spin-spin interactions; the presence of both symmetries has been discussed above. Superposed there is a lines sextet due to the hyperfine interaction between the electronic spin and the nuclear spin (I = 5/2). The hyperfine coupling constant A has values of 87, 89 and 90 G for 0.4, 1 and 2% Mn samples concentration, respectively. The increase of the coupling constant when Mn^{2+} concentration increases suggests the increase of the ionic character of the bonding between Mn^{2+} and the O^{2-} ions generated by the octahedral symmetry of the ligand field. When the concentration of Mn^{2+} ions increases beyond 2%, the hyperfine splitting sextet disappears leaving a single broad line due to the increase of the magnetic dipole-dipole interactions. The line width for 12% Mn concentration is Δ = 555 G with no hyperfine structure. The lack of the hyperfine splitting at these absorption lines could be due to the non-homogeneous ligand field in the Mn^{2+} neighborhood and the random distribution of the octahedral/tetrahedral distortions vicinity [27]. The resonances labeled as g = 3.3 and g = 4.3 are due to the superposition of the transitions between the Kramer's doublets $|S = \pm 1/2> \rightarrow |S = \pm 3/2>$ and $|S = \pm 3/2> \rightarrow |S = \pm 5/2>$ of octahedral and tetrahedral symmetries, smeared out because each one has different D and E values as well as different magnetic axes orientations due to the glassy structure [43].

4. Conclusions

Zinc phosphate glasses were synthesized at various molar compositions of phosphate and MnO. With the increase of MnO concentration occurs a modification of the local environment symmetry of Mn^{2+} ions from tetrahedral to an octahedral one; the PL spectra consist of several bands in the region from 400 nm to 700 nm which change by increasing both yellow and red emissions and a reduction of green emission as the Mn^{2+} ion concentration changes. The modification of coordination number was detected through techniques as Raman because of the reduction of the $(PO_2)_{asym}$, $(PO_2)_{sym}$, $(POP)_{sym}$ and bend mode vibrations suggesting a structural modification, and the EPR spectra by the increase of intensity of resonances on g = 2.0, 3.3 and 4.3. Crystalline phases of ZnO can be grown and segregated, during the synthesis of zinc phosphate glass whose presence influences the luminescence spectra by the addition of a blue emission centered at 420 nm. Therefore, an RGB luminescence spectrum is obtained where a blue-red emission happens by exciting with 350 nm light and a green-red emission happens by exciting with 409 nm light. The ratio between blue, green and red intensities could be changed by the control of Mn^{2+} local symmetry and the controlled growth of crystalline ZnO. Tunability of Mn^{2+} luminescence color from blue to red suggests applications as a changing phosphor in solid state lighting devices switching the excitation light wavelength.

Acknowledgments

To Cristina Zorrilla and Jorge Barreto for the technical support provided, and CONACyT for the financial support.

References

[1] A. Ghosh, Phys. Rev. B 42 (1990) 5665.
[2] I. Ardelean, P. Pascuta, Mod. Phys. Lett. B 15 (2001) 1445.
[3] S. Bhattacharya, A. Ghosh, Phys. Rev. B 68 (2003) 224202.
[4] T. Sankarappa, et al., J. Alloys Compd. 469 (2009) 576.
[5] A.A. Bahgat, et al., J. Alloys Compd. 506 (2010) 141.
[6] S. Sanghi, S. Duhan, A. Agarwal, P. Aghamkar, J. Alloys Compd. 488 (2009) 454.
[7] S.P. Singh, R.P.S. Chakradhar, J.L. Rao, B. Karmakar, Physica B 405 (2010) 2157.
[8] Y. Yu, et al., NPG Asia Mater. 8 (2016) e318.
[9] S. Zhou, N. Jiang, B. Wu, J. Hao, J. Qiu, Adv. Funct. Mater. 19 (13) (2009) 2081–2088.
[10] S. Zhou, et al. J. Am. Chem. Soc. 132 (50) (2010) 17945–17952.
[11] Y. Li, S. Zhou, G. Dong, M. Peng, L. Wondraczek, J. Qiu, Sci. Rep. 4 (2014) 4059(1)–4059(6).
[12] S. Zhou, J. Hao, J. Qiu, J. Am. Ceram. Soc. 94 (9) (2011) 2902–2905.
[13] S. Zhou, et al., Adv. Funct. Mater. 24 (43) (2013) 5436–5443.
[14] G. Nagarjuna, N. Venkatramaiah, P.V.V. Satyanarayana, N. Veeraiah, J. Alloys Compd. 468 (2009) 466.
[15] R.K. Singh, A. Srinivasan, J. Magn. Magn. Mater. 322 (2010) 2018.
[16] M. Cherian, M.S. Rao, A.M. Hirt, I.E. Wachs, G. Deo, J. Catal. 211 (2002) 482.
[17] X. Ge, M.M. Zhu, J.Y. Shen, React. Kinet. Catal. Lett. 77 (2002) 103.
[18] C.R. Kesavulu, et al., J. Alloys Compd. 496 (2010) 75.
[19] A. Ghosh, B.K. Chaudhuri, J. Non-Cryst. Solids 83 (1986) 151.
[20] A. Ghosh, J. Appl. Phys. 65 (1989) 227.

[21] N. Da, M. Peng, S. Krolikowski, L. Wondraczek, L. Opt. Express 18 (2010) 2549.
[22] Y. Won, H. Jang, W. Im, D. Jeon, Appl. Phys. Lett. 89 (2006) 231909.
[23] M. Kawano, H. Takebe, M. Kuwabara, Opt. Mater. 32 (2009) 277.
[24] G. Gao, S. Reibstein, M. Peng, L. Wondraczek, Phys. Chem. Glasses Eur. J. Glass Sci. Technol. B 52 (2) (2011) 59–63.
[25] G. Gao, N. Da, S. Reibstein, M. Peng, L. Wondraczek, L. Opt. Express 18 (2010) A557.
[26] M.S. Reddy, G.M. Krishna, N. Veeraiah, J. Chem. Solids 67 (2006) 789.
[27] P. Pascuta, M. Bosca, G. Borodi, E. Culea, J. Alloys Compd. 509 (2011) 4314–4319.
[28] R. Reisfeld, A. Kisilev, C.K. Jorgensen, Chem. Phys. Lett. 111 (1984) 150.
[29] K. Meyer, J. Non-Cryst. Solids 209 (1997) 227–239.
[30] R.K. Brow, D.R. Tallant, S.T. Myers, C.C. Phifer, J. Non-Cryst. Solids 191 (1995) 45.
[31] C.E. Smith, R.K. Brow, J. Non-Cryst. Solids 390 (2014) 51–58.
[32] A. Margaryan, J.H. Choi, F.G. Shi, Appl. Phys. B Lasers Opt. 78 (2004) 409–413.
[33] H.F. Quintero, J.A. Rocha, H.S. Murrieta, A.J. Hernández, G.E. Camarillo, J.M.C. Flores, C.A. Armenta, M.G. Hipólito, F.R. Brito, J. Lumin. 182 (2017) 107–113.
[34] D.H. Zhang, Q.P. Wang, Z.Y. Xue, Appl. Surf. Sci. 207 (2003) 20–25.
[35] D.M. Bagnall, Y.F. Chen, Z. Zhu, T. Yao, S. Koyama, M.Y. Shen, T. Goto, Appl. Phys. Lett. 70 (1997) 2230.
[36] M.J. Zheng, L.D. Zhang, G.H. Li, W.Z. Shen, Chem. Phys. Lett. 363 (2002) 123–128.
[37] W.C. Zhang, X.L. Wu, H.T. Chen, J. Zhu, G.S. Huang, J. Appl. Phys. 103 (2008) 093718.
[38] B.C. Taschendorf, T.M. Alam, R.T. Cygan, J.U. Otaigbe, J. Non-Cryst. Solids 316 (2003) 261–272.
[39] J.O. Rubio, E.P. Munoz, J.L. Boldu, Y. Chen, M.M. Abraham, J. Chern. Phys. 70 (1979) 633.
[40] R. Aasa, J. Chem. Phys. 52 (1970) 3919.
[41] I. Ardelean, S. Cora, R.C. Lucacel, O. Hulpus, Solid State Sci. 7 (2005) 1438.
[42] I. Ardelean, N. Muresan, P. Pascuta, Mod. Phys. Lett. B 20 (2006) 1607.
[43] V. Cern, B. Petrovh, M. Frumar, J. Non-Crys. Solids 125 (1990) 17–24.